AIP Advances

Transformational dynamics of BZO and BHO nanorods imposed by Y_2O_3 nanoparticles for improved isotropic pinning in $YBa_2Cu_3O_{7-\delta}$ thin films

Cite as: AIP Advances **7**, 075308 (2017); https://doi.org/10.1063/1.4991051
Submitted: 22 April 2017 . Accepted: 27 June 2017 . Published Online: 13 July 2017

Bibek Gautam, Mary Ann Sebastian, Shihong Chen, Jack Shi, Timothy Haugan, Zhongwen Xing, Wenrui Zhang, Jijie Huang, Haiyan Wang, Mike Osofsky, Joseph Prestigiacomo, and Judy Z. Wu

Transformational dynamics of BZO and BHO nanorods imposed by Y_2O_3 nanoparticles for improved isotropic pinning in $YBa_2Cu_3O_{7-\delta}$ thin films

Bibek Gautam,[1,a] Mary Ann Sebastian,[2] Shihong Chen,[1,3] Jack Shi,[1] Timothy Haugan,[2] Zhongwen Xing,[3] Wenrui Zhang,[4] Jijie Huang,[4] Haiyan Wang,[4] Mike Osofsky,[5] Joseph Prestigiacomo,[5] and Judy Z. Wu[1,b]

[1]*Department of Physics and Astronomy, University of Kansas, Lawrence, Kansas 66045, USA*
[2]*U.S. Air Force Research Laboratory, Aerospace Systems Directorate, WPAFB, OH 45433, USA*
[3]*College of Engineering and Applied Science, Nanjing University, Nanjing, Jiangsu 210093, China*
[4]*School of Materials Engineering, Purdue University, West Lafayette, IN 47907, USA*
[5]*US Naval Research Laboratory, 4555 Overlook Ave, SW Washington, DC 20375, USA*

(Received 22 April 2017; accepted 27 June 2017; published online 13 July 2017)

An elastic strain model was applied to evaluate the rigidity of the c-axis aligned one-dimensional artificial pinning centers (1D-APCs) in $YBa_2Cu_3O_{7-\delta}$ matrix films. Higher rigidity was predicted for $BaZrO_3$ 1D-APCs than that of the $BaHfO_3$ 1D-APCs. This suggests a secondary APC doping of Y_2O_3 in the 1D-APC/$YBa_2Cu_3O_{7-\delta}$ nanocomposite films would generate a stronger perturbation to the c-axis alignment of the $BaHfO_3$ 1D-APCs and therefore a more isotropic magnetic vortex pinning landscape. In order to experimentally confirm this, we have made a comparative study of the critical current density J_c (H, θ, T) of 2 vol.% $BaZrO_3$ + 3 vol.%Y_2O_3 and 2 vol.%$BaHfO_3$ + 3 vol.%Y_2O_3 double-doped (DD) $YBa_2Cu_3O_{7-\delta}$ films deposited at their optimal growth conditions. A much enhanced isotropic pinning was observed in the $BaHfO_3$ DD samples. For example, at 65 K and 9.0 T, the variation of the J_c across the entire θ range from θ=0 (H//c) to θ=90 degree (H//ab) is less than 18% for $BaHfO_3$ DD films, in contrast to about 100% for the $BaZrO_3$ DD counterpart. In addition, lower α values from the $J_c(H) \sim H^{-\alpha}$ fitting were observed in the $BaHfO_3$ DD films in a large θ range away from the H//c-axis. Since the two samples have comparable J_c values at H//c-axis, the improved isotropic pinning in $BaHfO_3$ DD films confirms the theoretically predicted higher tunability of the $BaHfO_3$ 1D-APCs in APC/$YBa_2Cu_3O_{7-\delta}$ nanocomposite films. [http://dx.doi.org/10.1063/1.4991051]

High temperature superconductors (HTSs) can have a strong impact on electrical applications including power cables, motors, generators, transformers, fault current limiters, and electromagnets. Many of these applications require high critical current density (J_c) at moderate to high magnetic fields of a few Teslas.[1–4] Generating strong artificial pinning centers (APCs) of desired morphology, dimension and concentration in HTS films and conductors has been a major focus of research during the past decade.[4–19] Exciting progress has been made via strain-mediated self-organization of nanoscale APCs of impurity phases in $YBa_2Cu_3O_{7-\delta}$ (YBCO) thin films and conductors.[20–22] Among others, c-axis aligned one-dimensional APCs (1D-APCs) have exhibited strong correlated pinning to magnetic vortices at magnetic field H//c-axis, resolving the issue of weak pinning along the c-axis originated from

[a]Corresponding author: Bibek Gautam, gautbibe@ku.edu
[b]jwu@ku.edu

the layered structure of the YBCO. Several materials have been reported to form c-axis aligned 1D-APCs in APC/YBCO nanocomposite films including $BaZrO_3$ (BZO), $BaSnO_3$ (BSO), and $BaHfO_3$ (BHO).[21–24] However, the perfectly aligned or small-angle splayed (~10° for BZO and ~13° for BHO at their optimal growth temperature of 810 °C - 830 °C) 1D-APCs may not benefit vortex pinning when H is oriented considerably away from the c-axis.[16,23,25] This results in prominent J_c peaks at H//c-axis (θ=0) and H//ab-plane (θ=90° due to the intrinsic pinning) separated by a low J_c valley at the θ angles in between. This J_c anisotropy with respect to the H orientations may be quantified using the normalized J_c variation between the highest J_c ($J_{c,max}$) at the larger of the J_c peaks and the lowest at the J_c valley by ($J_{c,max}$ - $J_{c,min}$)/$J_{c,min}$. For example: at 77 K, the J_c anisotropy is around 80.9% and 95.6%, respectively, at 1 T and 3 T in 2% BZO APC/YBCO nanocomposite films.[16] In order to achieve a more isotropic J_c, several APC structural control approaches have been explored including double-doping with a combination of 1D-APCs (BZO or BSO or BHO, $Ba_2(Y/Gd)(Nb/Ta)O_6$) and 0D-APCs (Y_2O_3, or $(Y/Gd)_2O_3$),[15,25–30] and length and splay control of 1D-APCs through alternate/segmented layer deposition.[31] These approaches indeed have reduced the J_c anisotropy compared to single doped YBCO thin films. Jha *et al* shows that the J_c anisotropy changed from 181% to 82.3% at 77 K and 1 T for 3.0 vol. % BSO +3.0 area % Y_2O_3/YBCO film as compared to 3% BSO/YBCO film.[32] The reduced J_c anisotropy could be attributed to the shorter length of 1D-APCs along the c-axis and suggests that the presence of the secondary APCs may provide a unique approach to control the morphology of the primary APCs for strong and isotropic pinning.[16,29]

In this paper, we illustrate the alignment of the BZO and BHO 1D-APCs, although having comparable diameters of ~5-7 nm,[33] can be tuned differently by the addition of secondary APCs of Y_2O_3 0D-APCs, leading to a different pinning landscape and hence J_c (H, θ) behaviors. It should be noted that BZO and BHO have subtle differences both in their lattice mismatches with the YBCO matrix and in their elastic properties. Based on an elastic strain model we developed recently in assessing the materials selection for 1D-APCs,[34] the lattice mismatch between APC and YBCO along with the elastic properties of both were found to affect the morphology of the APCs formed in the APC/YBCO nanocomposite films. By minimizing the elastic energy of the APC/YBCO nanocomposite film, a lattice mismatch vs. elastic constant phase boundary has been obtained between materials that can form c-axis aligned 1D-APCs and those that cannot.[34] Quantitatively, the rigidity of the c-axis aligned 1D-APCs should be proportional to its distance to the phase boundary. This means that the shorter the distance, the less rigidity is, and the more tunable the 1D-APCs would be by modification of the strain field. To confirm this hypothesis, this work has calculated the rigidity of the BZO and BHO 1D-APCs, and measured the transport $J_c(H)$ of YBCO films double-doped with BZO+Y_2O_3 (BZO DD) or BHO+Y_2O_3 (BHO DD), respectively. Remarkably, we have found that the BHO 1D-APCs have lower rigidity and confirmed experimentally that a stronger and more isotropic pinning can be obtained in the BHO DD case due to higher tunability of the BHO 1D-APC microstructures.

BZO DD (or BHO DD) samples with 2 vol. % BZO (or BHO) mixed with 3 vol. %Y_2O_3 were fabricated at 825 °C for BZO and 810 °C for BHO respectively, with oxygen partial pressure of 300 mTorr using pulsed laser deposition on (100) $SrTiO_3$ (STO) single crystal substrates. A Lambda Physik LPX 300 KrF excimer laser (248 nm) was utilized for the depositions at fluence of approximately 1.6 J/cm^2 on target and repetition frequency of 8.0 Hz. All samples were further annealed for 30 minutes at 500 °C within an oxygen atmosphere. The film thicknesses were determined using a Tencor profilometer, with an average thickness of 160 nm for BHO DD and 140 nm for BZO DD thin films.

For electrical transport measurements, samples with two parallel microbridges of 500 μm (length) x20 μm or 40 μm (width), respectively, were patterned using photolithography. Quantum Design Evercool II Physical Properties Measurement System (PPMS) with a vibrating sample magnetometer was employed for measuring T_c and the transport J_c (H, θ) as function of temperature T, magnetic field H (up to 9.0 T). Current-voltage characteristics were measured using Keithley 2430 1 KW pulsed current source meter and HP 34420. J_c was determined by applying the standard 1 μV/cm criterion.

Figure 1 shows the lattice mismatch $|f_1/f_3|$ vs. elastic constant phase diagram for several APC materials in YBCO matrix calculated using the elastic strain model.[34] The f_1 and f_3 represent

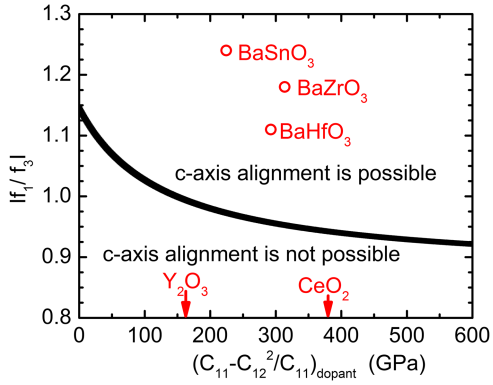

FIG. 1. Calculated (f_1/f_3) vs $(C_{11}\text{-}C_{12}^2/C_{11})_{dopant}$ phase boundary (solid line) above which the dopant materials energetically prefer to form c-axis aligned 1D-APCs in YBCO thin films. f_1 and f_3 are the lattice mismatch of film and dopants along a- and c-axes respectively. C_{11} and C_{12} are elastic constants of the dopant. The points for Y_2O_3 and CeO_2 are below the limit of the y-axis.

the lattice mismatch between the YBCO and APC dopant along [100] and [001] directions respectively. C_{11} and C_{12} are the elastic constants of the dopants. As illustrated in Figure 1, both BZO and BHO are above the phase boundary (solid line) separating the APC materials that energetically prefer to form the c-axis aligned 1D-APCs in YBCO from those, such as Y_2O_3 and CeO_2, that do not (below the phase boundary). Considering the APC morphology changes across the phase boundary, the smaller distance of the BHO towards the phase boundary than that of BZO (and BSO) indicates the rigidity of the BHO 1D-APCs is less than that of the BZO (BSO) counterparts. This means that the formation of the c-axis aligned BHO 1D-APCs could be more interrupted by the presence of the secondary dopant of Y_2O_3 0D-APCs. The consequence of the interruption is the deviation from perfect alignment of the 1D-APCs along the c-axis of YBCO as illustrated in the shortened length and broadened splay angle of the 1D-APCs. Hypothetically, shorter and more mis-oriented BHO 1D-APCs in the BHO DD samples could lead to a more 3D pinning landscape as compared to the BZO DD case.

High crystallinity was confirmed in the X-ray diffraction (XRD) θ-2θ spectra for the BZO DD (black) and BHO DD (red) samples. Both of them are c-axis-oriented with c-axis lattice constant of 1.172 nm BZO DD and 1.177 nm for BHO DD. These slightly larger c-axis lattice constants than that of the undoped YBCO film are expected from the coherent interfaces between the BZO (or BHO) with the YBCO matrix.[24,35,36] The insets of Figure 2a depict the XRD (005) rocking curves taken on

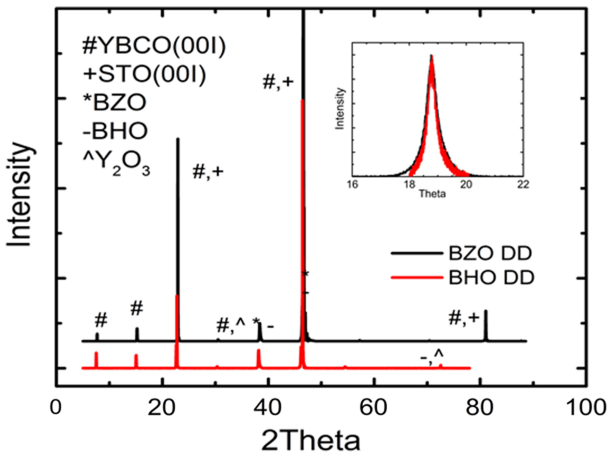

FIG. 2. XRD θ-2θ scan for 2 vol.% BZO+3 vol.% Y_2O_3 (BZO DD) and 2 vol.% BHO +3 vol.% Y_2O_3 (BHO DD) doped YBCO nanocomposite films on STO substrates. Insets: rocking curve of YBCO (005) peak of the same samples. Color codes are same for both figures.

the BZO DD and BHO DD samples, respectively. A considerably larger full-width-at a half maximum (FWHM) of the former (0.839 deg), than that of the latter (0.353 deg) indicates the YBCO lattice is disturbed (such as ab-plane buckling), considerably more in the BZO DD sample. This may explain its more severe T_c degradation to 85.71 K as compared to 87.08 K of the BHO DD sample (R-T curve Figure S2 of the supplementary material). Figure S1 of the supplementary material compares transmission electron microscopy (TEM) images taken on both BZO DD and BHO DD samples. In both cases, massive large nanoparticles of a several nanometers in diameter can be clearly seen in addition to the BZO and BHO 1D-APCs aligned in the c-axis of YBCO films. This confirms the mixed APC morphologies in the BZO DD samples reported earlier by Maiorov *et al* and a similar APC landscape in the BHO DD samples.

Figure 3 compares the $J_c(H)$ curves of the BZO DD and BHO DD samples at 77 K and 65 K, respectively, at θ=0° (H//c-axis), θ=90° (H//ab-plane), and θ=45° (H at the mid-point between the c-axis and ab-plane). At H//c-axis (Figure 3a), the c-axis aligned BZO 1D-APCs (or BHO 1D-APCs) are anticipated to provide strong correlated pinning at up to the so-called matching fields determined by the areal density of the 1D-APCs. This enhanced correlated pinning is typically illustrated in the smaller H-field susceptibility, or the low α values of $J_c(H) \sim H^{-\alpha}$,[25,37] as compared to α ~ 0.5 for the undoped YBCO.[38] At 77 K, the α value is ~0.49 for BZO DD and ~0.27 for the BHO DD sample, indicating more enhanced pinning in the latter. The α value of the BHO DD sample is ~0.27, which is considerably lower than that (~0.32) of the BHO SD sample,[39] indicative of the improved pining in the former. One possible explanation of the negligible lower pinning efficiency of the BZO 1D-APCs may be the lower T_c too close to 77 K at which $J_c(H)$ was measured. This same T_c effect may explain the lower $J_c(H)$ observed on the BZO DD sample at θ=45° (Figure 3b) and θ=90° (Figure 3c) at 77 K. At 77K and 1.0 T, J_c (H//c-axis) for the BHO DD (~0.24 MA/cm^2) is lower than ~ 7.0 mol % BZO + 7.0 mol%Y_2O_3 DD sample (0.45 MA/cm^2)[40] and 3 wt.% BZO+2 wt.% Y_2O_3 DD sample (0.4 MA/cm^2).[41] Although the J_c value in BHO DD sample is not superior to BZO DD,[41] the lower α value for BHO DD (0.27) compared BZO DD (0.31)[41] indicates the slightly stronger vortex pinning in the former. In addition, the higher H_{max} of ~3.5 T for BHO DD film as compared to BZO DD film's 3.0 T[41] indicates a higher concentration of strong APCs in the former.

This T_c effect becomes insignificant at 65 K, which is consistent with the comparable $J_c(H)$ curves observed on the two samples. At H//c-axis, the $J_c(H)$ for the BZO DD sample is even slightly higher than that of BHO DD sample in the field range of 0-9.0 T (Figure 3a). Moreover, comparable α values of 0.17 for BZO DD and 0.16 for BHO DD samples were obtained from the $J_c(H) \sim H^{-\alpha}$ fitting at H//c-axis. This suggests the most probable explanation for the slightly lower $J_c(H)$ in the BHO DD sample is the more disturbance of the BHO 1D-APC alignment in the c-axis. The effectively longer length of the former provides more effective pinning at H//c-axis and result in an overall higher $J_c(H)$ at 65 K.

The less c-axis alignment in the BHO DD case implies a possible enhanced pinning as H is not oriented at H//c-axis. Indeed, a higher $J_c(H)$ at $H \geq 2.0$ T for BHO DD sample was observed at 65 K at both θ=45° (Figure 3b) and θ=90° (Figure 3c) due to a crossover of the $J_c(H)$ curves

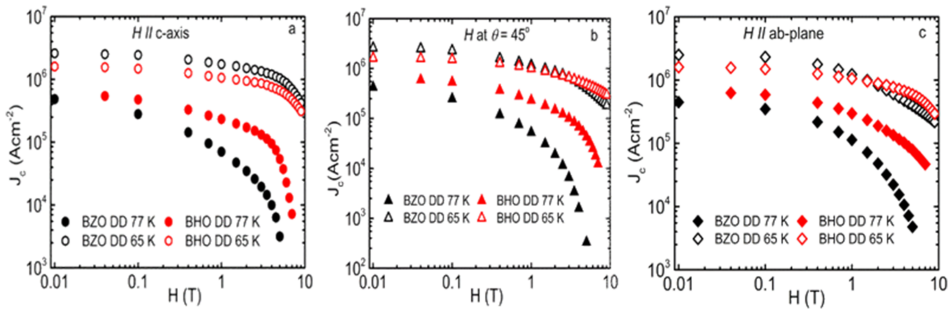

FIG. 3. J_c vs. H curves measured on BZO DD (black) and BHO DD (red) samples at (a) θ=0° (H//c-axis); (b) θ = 45°; and (c) θ = 90° (H//ab-plane) at 77 K (solid) and 65 K (open), respectively.

for these samples at ~ 2.0 T. The trends in the θ=45° and θ=90° cases indicate the BHO APCs enhance the pinning at *H*//ab-plane and also at angles in between the c-axis and ab-plane. This enhancement in such a wide angle range is unlikely associated to the small angle splay of the BHO 1D-APCs around the c-axis. Rather, we argue that the presence of the secondary Y_2O_3 0D-APCs affects the kinetic diffusion process during the BHO 1D-APCs formation along the c-axis, resulting in many shorter, misaligned segments of the BHO 1D-APCs. In a comparative study we did earlier on BZO SD and BZO DD cases, it was found that the BZO 1D-APC length can be reduced by a factor 2-3 from the former to the latter case at the same growth conditions.[16] In addition, the shorter segments of the 1D-APCs tend to misalign away from the c-axis. While a similar effect is expected to happen in the BHO DD case, the level of the misalignment could be more significant considering the lower rigidity of the BHO 1D-APCs than that of the BZO 1D-APCs as shown in Figure 1.

There are two benefits from less c-axis alignment of the 1D-APCs. First, it may result in reduced strain on the YBCO lattice, which seems consistent with the 1.3 K higher T_c observed on BHO DD sample as compared with its BZO DD. This leads to significantly higher $J_c(H)$ of BHO DD samples at higher temperatures, such as 77 K as shown in Figure 3. On the other hand, it provides isotropic pinning at other *H* orientations away from *H*//c-axis. Indeed, at 65 K, significantly lower α values of 0.25 (θ = 45°) and 0.19 (θ = 90°) were observed for the BHO DD sample compared to that of 0.36 and 0.39 for the BZO DD counterpart. In particular, this results in smaller anisotropy of the α value at different *H* orientations.

Figure 4 compares the pinning force density (F_p) calculated from $F_p = \boldsymbol{J_c} \times \boldsymbol{H}$ at 77 K and 65 K as function of *H* at different *H*-field orientations of θ=0°, 45° and 90°, respectively. All $F_p(H)$ curves exhibit a typical inverted bell shape. The H_{max} at the peak of the F_p ($F_{p,max}$) corresponds to the matching field associated to the areal density of the strong pins, such as BZO and BHO APCs, in this work. At θ=0° (Figure 4a), the H_{max} values for the BZO DD and BHO DD samples are comparable at both 77 K and 65 K. This suggests the concentrations BZO-1D APCs and BHO-1D APCs aligned in the c-axis are reasonably close to each other. However, the $F_{p,max}$ value of 52.48 GN/m^3 for BZO DD film is about 1.5 times higher than that of the BHO DD counterpart at 65 K, at which point the T_c effect is negligible. The comparable H_{max} and higher $F_{p,max}$ values in the former confirm our earlier argument on the effectively longer length of the c-axis aligned BZO 1D-APCs.

This trend is certainly altered at θ=45° and 90° as shown in Figures 4b and 4c. In both cases, higher H_{max} and $F_{p,max}$ values were observed on BHO DD films at both 77 K and 65 K. At 65 K and at θ=45°, the H_{max} ~ 8.5 T in the BHO DD film is more than twice of the ~4.0 T for the BZO DD film (Figure 4b). In addition, the $F_{p,max}$~26.71 GN/m^3 for the BHO DD sample is 1.14 times higher than that of 22.43 GN/m^3 for the BZO DD counterpart. Since a similar behavior occurs also at *H*//ab-plane (Figure 4c), the stronger pinning in the BHO DD case may be attributed most probably to the shorter, misaligned BHO APCs. Inset of Figure 4b shows that the $F_{p,max}$ and H_{max} both increase monotonically with the decreasing temperatures for BHO DD sample at θ=0° and θ=45°. The comparable $F_{p,max}$ values (black) at these two angles in the temperature range of 50-77K, suggests BHO APCs, instead of the Y_2O_3 0D-APCs, are probably the dominant pinning centers

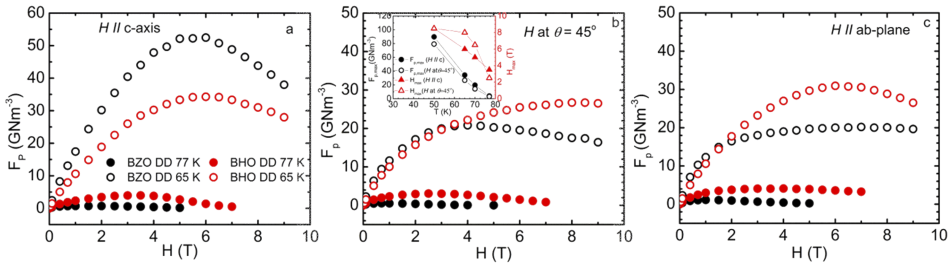

FIG. 4. F_p vs. *H* curves for BHO DD (red) and BZO DD (black) films at (a) θ=0° (*H*//c-axis), (b) θ = 45°; and (c),θ = 90° (*H*//ab-plane) at 77 K (solid) and 65 K (open), respectively. Insets: Temperature dependence of $F_{p,max}$ (circle) and H_{max} (triangle) measured on BHO DD at *H*//c-axis (solid), and *H* at θ = 45° (open). The connecting lines are for eye catching purpose.

in the BHO DD samples at different H orientations. Much larger H_{max} values were observed at 70 K or lower temperatures at θ=45° as compared to the θ=0° case, although a higher H_{max} was observed in the latter at 77 K. This trend indicates a larger number of smaller sizes BHO APCs are present in the BHO DD sample. These unaligned, smaller-size BHO APCs pin more strongly at lower temperatures. Remarkably, the H_{max} saturates at 8.5 T at 50 K in both orientations of θ=0° and 45°. These results illustrate the tunability of the c-axis alignment of the BZO and BHO 1D-APCs by the Y_2O_3 0D-APCs differs quantitatively due to the different rigidity of the BZO 1D-APCs and BHO 1D-APCs. The weaker rigidity in the latter enables a more significant disturbance of the 1D-APCs alignment to allow the BHO APCs to form in a more isotropic pinning landscape.

This argument is supported by the more isotropic $J_c(\theta)$ curves observed on BHO DD samples as compared to the BZO DD ones at both 77 K (Figure 5a) and 65 K (Figure 5b). A major difference is in the absence of the J_c valley as θ is in between θ=0° and θ=90° for the BHO DD samples. The appearance of the J_c valley is the consequence of weaker pinning in this angle range as compared to the stronger pinning at θ=0 due to the aligned 1D-APCs and at θ=90° due to the ab-plane intrinsic pinning. This leads to the J_c anisotropy with respect to H orientations and the larger the difference between the J_c peaks and valley as in most 1D-APC/YBCO nanocomposites, the larger the J_c anisotropy.[16,39] For example, the J_c anisotropy is about 100% for 2.0 vol.% BZO SD films at 77 K and 1.0 T,[16] which is similar to the 3.0 vol.% BSO SD case.[32] However, higher J_c anisotropy of 159.0% for BZO DD with $J_{c,min}$= 0.59*10^5 A/cm^2 in this study suggests most BZO 1D APCs remained aligned in the c-axis in the 2.0 vol.% BZO DD samples. An opposite trend was observed in comparison of BHO SD and DD samples. At 77 K and H=1.0 T, the overall $J_c(\theta)$ values for the entire angular range from θ=0° (H//c-axis) to θ=90° (H//ab-plane) are higher in the BHO DD film than in the BHO SD film.[39] In addition, the J_c anisotropy is about 41% for the BHO DD film, which is about a half of ~80% for the BHO SD film.[42] This result seems consistent with the higher orientation tunability of the BHO 1D-APCs in the DD case predicted in Fig. 1. The J_c anisotropy is about 40% for the BHO DD samples measured at 77 K at 1 T. The anisotropy reduces further to about 18% for the BHO DD films at 65 K and 9.0 T (red diamonds), in contrast to about 100% for the BZO DD counterpart (black diamonds) as shown in Figure 5b. This result illustrates the importance of engineering the APC morphology and orientation.

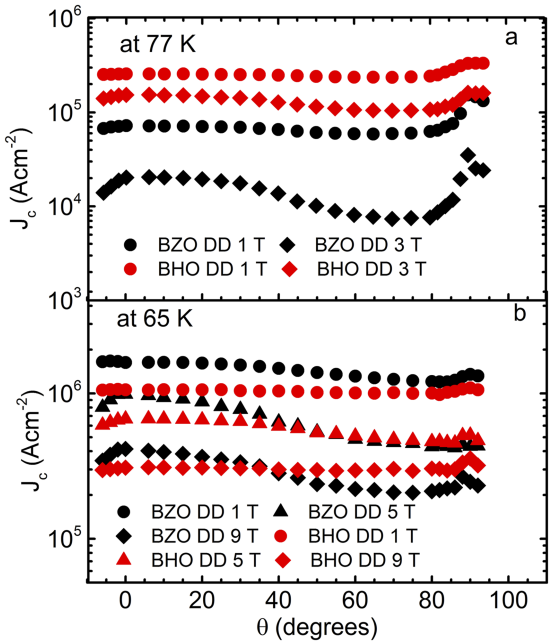

FIG. 5. Angular dependence of J_c measured on BHO DD (red) and BZO DD (black) thin film (a) at 1 T (circle) and 3 T (diamond) at 77 K (b) 1 T (circle), 5 T (triangle) and 9 T (diamond) at 65 K.

In summary, a comparative study has been carried out to probe the tunability of the BZO and BHO 1D-APCs alignment along the c-axis by a secondary Y_2O_3 0D-APCs in BZO DD/YBCO and BHO DD/YBCO nanocomposite films. Since this tunability correlates to the microstructure of the APCs, which in turn affects the J_c anisotropy with respect to the H orientations, transport J_c was measured in the temperature range of 50-77 K at H up to 9.0 T, and different H orientations. The experimentally observed higher tunability of the BHO APCs by the Y_2O_3 0D-APCs seems to agree well with the theoretically predicted lower rigidity of the BHO 1D-APCs as compared to the BZO 1D-APC counterpart's, and lead to achievement of much smaller J_c anisotropy due to formation of short, unaligned BHO APCs that enhance pinning at most H orientations.

SUPPLEMENTARY MATERIAL

See supplementary material for the Transmission Electron Microscopy (TEM) images of the BZO DD and BHO DD samples, and R-T curve with detail description.

ACKNOWLEDGMENTS

This research was supported in part by NSF contracts Nos: NSF-DMR-1337737 and NSF-DMR-1508494, the AFRL Aerospace Systems Directorate, and the Air Force Office of Scientific Research (AFOSR), the US National Science Foundation (DMR-1565822) for TEM characterization.

[1] R. Teranishi, K. Otaguro, H. Horita, K. Yamada, K. Kaneko, T. Izumi, and S. Awaji, IEEE Transactions on Applied Superconductivity **26**(3), 1–3 (2016).
[2] X. Obradors and T. Puig, Superconductor Science and Technology **27**(4), 044003 (2014).
[3] A. P. Malozemoff, Nature Materials **6**(9), 617 (2007).
[4] S. Foltyn, L. Civale, J. MacManus-Driscoll, Q. Jia, B. Maiorov, H. Wang, and M. Maley, Nature Materials **6**(9), 631–642 (2007).
[5] K. Matsumoto and P. Mele, Superconductor Science and Technology **23**(1), 014001 (2009).
[6] Y. Yoshida, K. Matsumoto, M. Miura, Y. Ichino, Y. Takai, A. Ichinose, M. Mukaida, and S. Horii, Physica C: Superconductivity and its Applications **445**, 637–642 (2006).
[7] P. Barnes, J. Kell, B. Harrison, T. Haugan, C. Varanasi, M. Rane, and F. Ramos, Applied Physics Letters **89**(1), 012503 (2006).
[8] T. J. Haugan, P. N. Barnes, T. A. Campbell, N. A. Pierce, F. J. Baca, and I. Maartense, IEEE Transactions on Applied Superconductivity **17**(2), 3724–3728 (2007).
[9] S. Harrington, J. Durrell, B. Maiorov, H. Wang, S. Wimbush, A. Kursumovic, J. Lee, and J. MacManus-Driscoll, Superconductor Science and Technology **22**(2), 022001 (2008).
[10] C. Varanasi, J. Burke, H. Wang, J. Lee, and P. Barnes, Applied Physics Letters **93**(9), 092501 (2008).
[11] J. Gutierrez, A. Llordes, J. Gazquez, M. Gibert, N. Roma, S. Ricart, A. Pomar, F. Sandiumenge, N. Mestres, and T. Puig, Nature Materials **6**(5), 367–373 (2007).
[12] S. Kang, A. Goyal, J. Li, A. A. Gapud, P. M. Martin, L. Heatherly, J. R. Thompson, D. K. Christen, F. List, and M. Paranthaman, Science **311**(5769), 1911–1914 (2006).
[13] K. Matsumoto, T. Horide, K. Osamura, M. Mukaida, Y. Yoshida, A. Ichinose, and S. Horii, Physica C: Superconductivity **412**, 1267–1271 (2004).
[14] G. Hammerl, A. Schmehl, R. Schulz, B. Goetz, H. Bielefeldt, C. Schneider, H. Hilgenkamp, and J. Mannhart, Nature **407**(6801), 162–164 (2000).
[15] S. Chen, M. Sebastian, B. Gautam, J. Wilt, T. Haugan, Z. Xing, and J. Wu, IEEE Transactions on Applied Superconductivity **27**(4), 1–5 (2017).
[16] J. F. Baca, T. J. Haugan, P. N. Barnes, T. G. Holesinger, B. Maiorov, R. Lu, X. Wang, J. N. Reichart, and J. Z. Wu, Advanced Functional Materials **23**(38) (2013).
[17] T. Aytug, M. Paranthaman, A. A. Gapud, S. Kang, H. M. Christen, K. J. Leonard, P. M. Martin, J. R. Thompson, D. K. Christen, and R. Meng, Journal of Applied Physics **98**(11), 114309 (2005).
[18] D. Abraimov, A. Ballarino, C. Barth, L. Bottura, R. Dietrich, A. Francis, J. Jaroszynski, G. Majkic, J. McCallister, and A. Polyanskii, Superconductor Science and Technology **28**(11), 114007 (2015).
[19] V. Selvamanickam, M. H. Gharahcheshmeh, A. Xu, E. Galstyan, L. Delgado, and C. Cantoni, Applied Physics Letters **106**(3), 032601 (2015).
[20] S. Miura, Y. Yoshida, Y. Ichino, Y. Doki, A. Ibi, T. Izumi, and T. Kato, IEEE Transactions on Applied Superconductivity **26**(4), 1–5 (2016).
[21] J. Wu, J. Shi, F. Baca, R. Emergo, J. Wilt, and T. Haugan, Superconductor Science and Technology **28**(12), 125009 (2015).
[22] X. Obradors, T. Puig, S. Ricart, M. Coll, J. Gazquez, A. Palau, and X. Granados, Superconductor Science and Technology **25**(12), 123001 (2012).
[23] M. Erbe, J. Hänisch, R. Hühne, T. Freudenberg, A. Kirchner, L. Molina-Luna, C. Damm, G. Van Tendeloo, S. Kaskel, and L. Schultz, Superconductor Science and Technology **28**(11), 114002 (2015).
[24] J. Z. Wu, J. J. Shi, J. F. Baca, R. Emergo, T. J. Haugan, B. Maiorov, and T. Holesinger, Superconductor Science and Technology **27**(4), 044010 (2014).

[25] T. Horide, T. Kawamura, K. Matsumoto, A. Ichinose, M. Yoshizumi, T. Izumi, and Y. Shiohara, Superconductor Science and Technology **26**(7), 075019 (2013).
[26] M. A. P. Sebastian, J. N. Reichart, M. M. Ratcliff, T. J. Bullard, J. L. Burke, C. R. Ebbing, G. Y. Panasyuk, C.-F. Tsai, W. Zhang, and J. Huang, IEEE Transactions on Applied Superconductivity **27**(4), 1–5 (2017).
[27] V. Selvamanickam, M. H. Gharahcheshmeh, A. Xu, Y. Zhang, and E. Galstyan, Superconductor Science and Technology **28**(7), 072002 (2015).
[28] G. Ercolano, M. Bianchetti, S. Wimbush, S. Harrington, H. Wang, J. Lee, and J. MacManus-Driscoll, Superconductor Science and Technology **24**(9), 095012 (2011).
[29] B. Maiorov, S. A. Baily, H. Zhou, O. Ugurlu, J. A. Kennison, P. C. Dowden, T. G. Holesinger, S. R. Foltyn, and L. Civale, Nature Materials **8**(5), 398–404 (2009).
[30] A. K. Jha, K. Matsumoto, T. Horide, S. Saini, P. Mele, A. Ichinose, Y. Yoshida, and S. Awaji, IEEE Transactions on Applied Superconductivity **26**(3) (2016).
[31] K. Matsumoto, T. Horide, A. K. Jha, P. Mele, Y. Yoshida, and S. Awaji, IEEE Transactions on Applied Superconductivity **25**(3), 1–6 (2015).
[32] A. K. Jha, K. Matsumoto, T. Horide, S. Saini, P. Mele, Y. Yoshida, and S. Awaji, IEEE Transactions on Applied Superconductivity **25**(3), 1–5 (2015).
[33] H. Tobita, K. Notoh, K. Higashikawa, M. Inoue, T. Kiss, T. Kato, T. Hirayama, M. Yoshizumi, T. Izumi, and Y. Shiohara, Superconductor Science and Technology **25**(6), 062002 (2012).
[34] J. J. Shi and J. Z. Wu, Philosophical Magazine **92**(23), 2911–2922 (2012).
[35] R. Guzman, J. Gazquez, V. Rouco, A. Palau, C. Magen, M. Varela, J. Arbiol, X. Obradors, and T. Puig, Applied Physics Letters **102**(8), 81906 (2013).
[36] A. Llordes, A. Palau, J. Gázquez, M. Coll, R. Vlad, A. Pomar, J. Arbiol, R. Guzman, S. Ye, and V. Rouco, Nature Materials **11**(4), 329–336 (2012).
[37] G. Blatter, M. V. Feigel'man, V. B. Geshkenbein, A. I. Larkin, and V. M. Vinokur, Reviews of Modern Physics **66**(4), 1125 (1994).
[38] V. Matsui, V. Flis, V. Moskaliuk, A. Kasatkin, N. Skoryk, and V. Svechnikov, J. Nanosci. Nanoeng. **1**(2), 38–43 (2015).
[39] P. Pahlke, M. Lao, M. Eisterer, A. Meledin, G. Van Tendeloo, J. Hänisch, M. Sieger, A. Usoskin, J. Strömer, and B. Holzapfel, IEEE Transactions on Applied Superconductivity **26**(3), 1–4 (2016).
[40] F. Ding, H. Gu, T. Zhang, H. Wang, F. Qu, S. Dai, X. Peng, and J. Cao, Journal of Alloys and Compounds **513**, 277–281 (2012).
[41] P. Mele, K. Matsumoto, T. Horide, A. Ichinose, M. Mukaida, Y. Yoshida, S. Horii, and R. Kita, Superconductor Science and Technology **21**(1), 015019 (2007).
[42] M. Sieger, P. Pahlke, M. Lao, M. Eisterer, A. Meledin, G. Van Tendeloo, R. Ottolinger, J. Hänisch, B. Holzapfel, and A. Usoskin, IEEE Transactions on Applied Superconductivity **27**(4), 1–7 (2017).